JOURNAL OF SPACECRAFT AND ROCKETS
Vol. 45, No. 1, January–February 2008

Sloshsat Spacecraft Calibration at Stationary Spin Rates

Jan P. B. Vreeburg*
2314 EX Leiden, The Netherlands

DOI: 10.2514/1.30975

Sloshsat Facility for Liquid Experimentation and Validation in Orbit was a spacecraft for the experimental study of the behavior of a contained liquid in space. It was launched from Kourou in French Guyana on Ariane 5 ECA on 12 February 2005. The free-flying mass was 129 kg, including 33.5 kg of liquid water in an 87 l tank. Control was by a set of 12 cold-gas thrusters with a thruster force of 0.785 N. The motion sensing subsystem had six linear accelerometers (Allied Signal QA-3000-010) in three pairs at different corners of the spacecraft, and three fiber optic gyroscopes (Litef μFORS 36/6). From the flight record, about 26 h of motion sensing subsystem data have been selected with Sloshsat in stable rotation, about its major axis of inertia at spin rates up to 6 rpm. The data have been used for the in-orbit calibration of the accelerometers and the determination of the spacecraft inertial properties. From the measurement equations of the six accelerometers, an error equation is derived for the six components of corrections to the system center of mass location and the angular rate vectors. The bias and scale factors for each accelerometer are determined to minimize the magnitude of the residual error. The procedure yields a 1σ value of $\mathcal{O}(5 \times 10^{-6}\ \mathrm{m/s^2})$ for the uncertainty of steady accelerometer data in a 30 mg range. The iterated angular rate data show much more resolution than the noisy output from the gyroscopes. The system inertia tensor at small nutation has been estimated under the assumption that the liquid is in hydrostatic equilibrium. Its six independent components have been separated in three principal moments of inertia and three variables of the orthogonal orientation tensor. The precision of the estimated principal moment of inertia values is thought to be $\mathcal{O}(1\%)$, based also on simulations of a Sloshsat-like system and realistic errors. The magnitudes of force and torque from leaking propulsion gas have been identified and were found to be of no special relevance for the calibration. The effects of geometrical errors in the mounting of the motion sensing subsystem sensors are estimated to be insignificant for the 1σ values as determined by the calibration.

Nomenclature

A, B, C = minor, intermediate, major moment of inertia, $\mathrm{kg \cdot m^2}$

$A2(x, y)$ = $\begin{bmatrix} x & y \\ -y & x \end{bmatrix}$

a = constant spin acceleration/$(2W_0)$, 1/s

$a_{\mathrm{cf}}, a_{\mathrm{err}}, a_{\mathrm{in}}, a_n, a_{\mathrm{out}}, a_p$ = accelerometer data, $\mathrm{m/s^2}$

$\boldsymbol{d}_C$ = Sloshsat system center of mass, m

$\mathrm{diag}(x, y)$ = $\begin{bmatrix} x & 0 \\ 0 & y \end{bmatrix}$

$\mathrm{diag}(A, B, C)$ = $\begin{bmatrix} A & 0 & 0 \\ 0 & B & 0 \\ 0 & 0 & C \end{bmatrix}$

E_1 = $[BW_0/(C-A)]^{1/2}$

E_2 = $[AW_0/(C-B)]^{1/2}$

$\boldsymbol{e}_i$ = unit vector along principal axis

g = gravity, 9.80708 $\mathrm{m/s^2}$

i = $(-1)^{1/2}$

$J_{3\times3}$ = $\begin{bmatrix} \mathbf{e_1} & \mathbf{e_2} & \mathbf{e_3} \end{bmatrix} \mathrm{diag}(A, B, C) \begin{bmatrix} \mathbf{e_1} & \mathbf{e_2} & \mathbf{e_3} \end{bmatrix}^T =$ Sloshsat inertia tensor

m = $W_0 m_1/E_1 + iW_0 m_2/E_2$

$\mathbf{m}$ = $\begin{bmatrix} m_1 & m_2 & m_3 \end{bmatrix}^T$ = fractional deviation of rotation rate from uniform spin W_0

n = sW_0 = nutation rate, rad/s

$\mathbf{Q}, \mathbf{Q_0}, \mathbf{U}$ = orthogonal matrices

R = length of $\boldsymbol{R}$, m

$\boldsymbol{R}$ = location vector, from origin at location $\mathbf{0}$, m

r = $\{B(C-B)/[A(C-A)]\}^{1/2} = E_1/E_2$

$\boldsymbol{r}$ = direction of $\boldsymbol{R}$

s = $[(C-A)(C-B)/(AB)]^{1/2}$

$\boldsymbol{s}$ = sensitive direction of accelerometer

T = accelerometer temperature, °C

T_b = temperature of the motion sensing subsystem electronics box, °C

t = time, s

$\boldsymbol{t}$ = $\{\boldsymbol{s}\}\boldsymbol{r}/\sin\varphi$, a unit vector

u = $t + at^2$

$\{\boldsymbol{v}\} = \begin{bmatrix} 0 & -v_3 & v_2 \\ v_3 & 0 & -v_1 \\ -v_2 & v_1 & 0 \end{bmatrix}$ = skew-symmetric matrix of vector $\boldsymbol{v}$, e.g., $\{\boldsymbol{v}\}r = v \times r$

W, W_0 = spin rate, rad/s

$\boldsymbol{W}$ = angular rate,rad/s

$\boldsymbol{\Delta} = [\Delta_b \Delta_\alpha \Delta_\beta \Delta_\pi \Delta_\sigma]^T$ = accelerometer error vector

$\boldsymbol{\varepsilon}$ = vector of small magnitude

$\boldsymbol{\sigma}(\boldsymbol{R})$ = acceleration at location $\boldsymbol{R}$, $\mathrm{m/s^2}$

$\boldsymbol{\tau}$ = torque, $\mathrm{N \cdot m}$

φ = angle, rad

ψ = $\tau_1/(AE_1) + i\tau_2/(BE_2) = \psi_0 e^{i\varphi}$

Ω = tank rotation rate magnitude, rad/s

$\boldsymbol{\Omega}$ = tank rotation rate, rad/s

$\boldsymbol{\Omega}_{\mathrm{mean}}$ = rate averaged over nutation cycles, rad/s

Received 12 March 2007; revision received 6 August 2007; accepted for publication 9 August 2007.

*Consultant, Gerbrandylaan 23; jan.vreeburg@gmail.com.

$\boldsymbol{\Omega}'$ = tank angular acceleration, rad/s^2
$\mathbf{1}_{3\times3}$ = identity matrix = diag(1, 1, 1)
$\mathcal{O}$ = order of magnitude

Superscripts

$'$ = time derivative d/dt, 1/s
T = transpose

Introduction

A PROPOSAL, in 1989, to ESA for the realization of a spacecraft to study slosh phenomena in space resulted in the Sloshsat spacecraft [1]. It was finally launched on an Ariane 5 ECA on 12 February 2005. Figure 1 shows a model with the important subsystems, including ESAject, a spring-loaded ejection system, and the communication hardware. The spacecraft was operated in geostationary transfer orbit from the Diane ground station at the launch site, using the 15-m-diam tracking antenna. The operational life of Sloshsat lasted ten passes and ended with the exhaust of the last propulsion gas on 21 February 2005. Each pass took between 6 and 9 h except for pass_03 and 04 which lasted 3.5 h each, separated by 2.5 h, and pass_05 which provided only 15 min of data as Sloshsat went through its perigee. Data have been collected during about 57.5 h of operations, which included a variety of maneuvers with large and small motions of the spacecraft [2]. The number following "pass_" gives its chronological order in the sequence of ten passes.

The Sloshsat system included tank instrumentation for diagnosis of liquid distribution and flowfield, the motion sensing subsystem (MSS) for determination of the spacecraft dynamic state, and sensors for housekeeping data (temperature, pressure, voltage, etc.). The data from the tank instrumentation were not received, a major mission anomaly that made it more difficult for the fluid dynamics scientists in the investigators' working group to validate their computational fluid dynamics (CFD) predictions of the liquid behavior [3]. Investigators from the two other disciplines in the investigators' working group, dynamic model construction and control algorithm development, have been affected less. A second anomaly was a small leak in the high-pressure part of the cold-gas system that feeds the 12 thrusters of 0.785 N force each. It started at the opening of the second tank of propulsion gas and caused accelerations of the system. An estimate of the magnitude of the leakage torque is important because it adds to the damping torque from viscous action in the water. The remaining source for scientific evaluation of the mission results was the data from the MSS. These include the output of six linear accelerometers that are located in three pairs at different corners of the Sloshsat box structure, and the record from a set of three orthogonal solid-state gyroscopes. It is known that the 1 g loading from terrestrial gravity inhibits accurate prediction of accelerometer performance under microgravity conditions [4] which makes on-orbit calibration necessary.

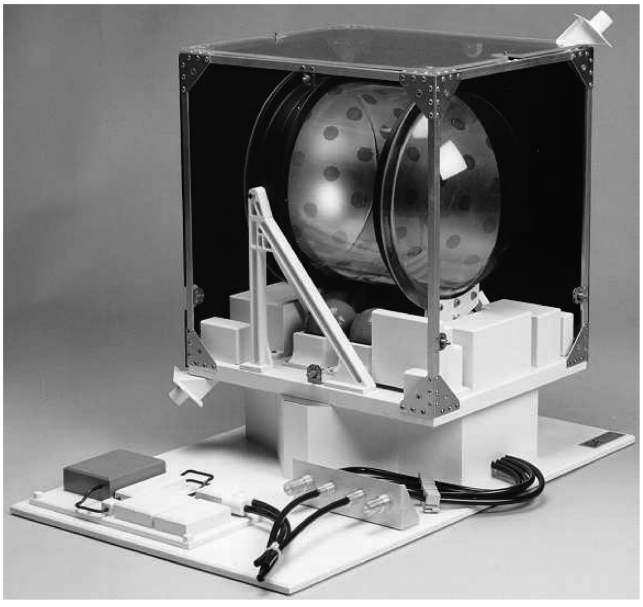

Fig. 1 Mock-up of Sloshsat FLEVO with its main subsystems.

One of the major aims of Sloshsat is the measurement of the force and torque from the liquid pressure field in its tank. In addition to the MSS, this measurement requires the knowledge of the inertial properties (mass, center of mass location, and inertia tensor) of the dry system. During the development of Sloshsat, much effort was devoted to the precise measurement of these properties and of the geometry of the MSS. The flight with Ariane 5 ECA required some structural changes from its original configuration which was qualified for flight on the Space Transportation System. The effect of these changes on the inertial properties has to be calculated because, for various reasons, measurement was no longer feasible except for the free-flying mass of 129 kg (including 33.5 kg of liquid water in the 87 l tank).

To provide necessary reference data to investigators, Sloshsat data have been processed and are used to determine the accuracy of the sensors, the magnitude of the leakage force and torque, and the Sloshsat inertial properties. The present paper reports on the methodology used to meet these objectives and the results. More reference data could have been provided for the benefit of future users of the Sloshsat results, e.g., an estimate of leakage force and torque over the full life span of Sloshsat, or the dry Sloshsat inertial properties as calculated from reconfiguration log entries. However, such work requires additional data collection and analysis which is outside the scope of the present effort.

The paper is organized in sections. It starts with an introduction to the methods that have been used for calibrations performed in the paper. After a description of the MSS, the data preprocessing is explained and is followed by selection of the calibration data set. The theory that supports the various calibration calculations is explained and is next applied to the Sloshsat case. This results section includes estimates of errors and estimates of the magnitudes of the torque and force due to gas leakage from the spacecraft. Conclusions on methodology and systems architecture are formulated.

Calibration basics

The calibration is performed with data taken during near-steady states of Sloshsat, i.e., a state of small nutation with the liquid configuration hydrostatic and calculable. The system is treated as rigid, with the liquid expression simplified to small changes of inertial properties with angular rate. The procedure is started by correction of the raw data for instrument errors from bus voltage drops, bias, and thermal effects. The calibration is then performed in two steps:

1) The MSS data are averaged over an integer number of nutation periods to nullify the nutation modulation. The data from the six accelerometers are processed to yield angular rate and system center of mass location.

2) A simple analytical solution of Euler's equations with constant torque is compared with a least-squares approximation to the components of the Sloshsat angular rate. The coefficients of the functional form of the solution provide a set of (nonlinear) equations that are used to solve for the inertia tensor and the torque.

The determination of the kinematical state of an arrangement of linear accelerometers [5] has a long history, but practical applications are limited to special problems such as the determination of the motion of collision dummies or of an object near an explosion. Many realizations use nine sensors in a special arrangement, whereas others use 12. The minimum configuration uses six [6]. The evaluation of the motion is often performed by elimination of the linear acceleration and the angular rate from the equations and solving for the angular acceleration. Integration generally results in a rapid divergence of the calculated angular rate, hence the limitation of the instrument to short-duration phenomena. With a set of nine accelerometers, both linear and angular accelerations can be

eliminated, leaving a system of nonlinear equations for the angular rate components. Solution of that system is problematic at certain rate values where the sign of a component becomes ambiguous. The combination of sensors in the MSS provides redundant data on its kinematical state without these known difficulties, and an assessment of its overall performance is intended later when all Sloshsat maneuvers have been evaluated. If the state of the arrangement is known, knowledge of its configuration allows determining its center of rotation, i.e., the location of the center of mass (c.m.) of the Sloshsat system.

The identification of the inertia tensor of a rigid spacecraft from a record of its angular rate requires a set of equations that predict measurement values. The parameters in these equations are functions of the inertia properties and are generally determined by a least-squares solution [7] of the comparison between predicted and recorded data. The choice of equations is wide but those based on conservation laws are preferred. Thus, for a rigid spacecraft and no external torque, conservation of (rotational) energy can be expressed, whereas spacecraft with wheels exploit conservation of angular momentum [8,9]. Integration of the equations of motion, in particular Euler's equations, leads to predictions of measured data like angular rate or attitude [10,11]. This approach is particularly attractive if an analytical solution [12–14] is valid because then the functional form of the time history is known. The inertia tensor components are solved from coefficients that are determined by a least-squares match of the known functional form to the data history. The analysis in the present paper is of this type. Different from the referenced analyses, the present one separates the six unknown components of the inertia tensor in principal moments of inertia (three) and the parameters (three) of the orthogonal tensor that describes the orientation of the principal axes in the spacecraft axes system. Because the inertia tensor is known approximately, errors are small quantities. The selection of the equations is influenced also by the accuracy of the sensor data, the a priori knowledge of the inertial properties, and whether data are to be processed recursively or in batch [15]. Important is whether maneuvers require thruster activation or if the spacecraft is coasting. For active maneuvers, a precise knowledge of thruster performance is necessary. In the present paper, no active maneuvers are considered but (constant) torque on the system is identified. Tanygin and Williams [7] provide a discussion on applicable techniques and data requirements starting from a generic expression of the equation to be solved. Inertia tensor identification is a problem also in fields other than space engineering, e.g., robotic handling of packages for postal service. A limited review of the literature did not bring information relevant to the problems discussed here. It is advisable to compare different options for analysis by the numerical results of simulations.

Motion Sensing Subsystem

The satellite is equipped with six linear accelerometers, in three pairs, and with three fiber optic gyroscopes that are mounted orthogonally on the MSS electronics box. A sketch of the configuration is given in Fig. 2. The maximum values of seismic point coordinates from origin O_M are $\begin{bmatrix} 617 & 505 & 625 \end{bmatrix}$ mm. The system c.m. is fairly near the center of the figure. The long arrow with the text "Sensor i," where i is a numeral, is the positive input axis of the accelerometer; the small arrow indicates the pendulous axis of the sensor. The sensitive directions are nominally along the axes of the Sloshsat coordinate system $\{XYZ\}_S$. The X_S axis is along the tank center line, the Z_S axis is along the ejection direction (see also Fig. 1), and the Y_S axis is approximately along the major axis of inertia $\boldsymbol{e}_3$. The principal axes triad is almost parallel to $\{XYZ\}_S$ with the axis of minimum inertia $\boldsymbol{e}_1$ near the Z_S axis. The positions of locations on the spacecraft are measured, with accuracy better than 0.01 mm maximum error, using a three-dimensional measurement table at ESA-Estec in Noordwijk, The Netherlands, with the following results [16]:

1) The location of each MSS accelerometer (and its effective c.m. of the proof-mass seismic elements) is determined with respect to the Sloshsat Facility for Liquid Experimentation and Validation in Orbit

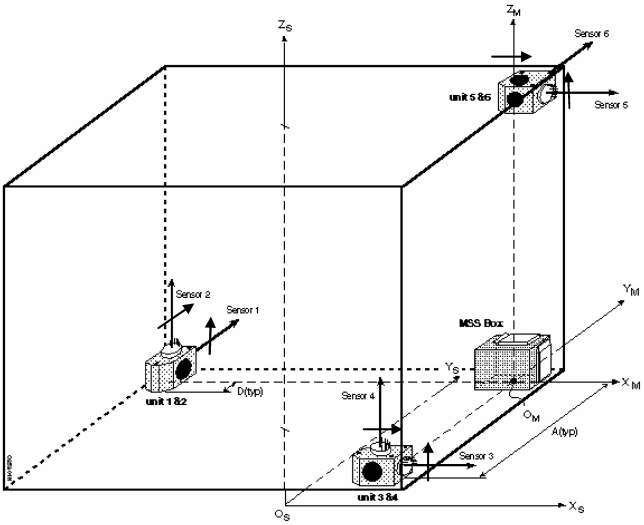

Fig. 2 The measurement coordinate system $\{XYZ\}_M$ in satellite system $\{XYZ\}_S$.

(FLEVO) coordinate system with accuracy better than 1 mm maximum error.

2) The orientation of the sensitive axis of each MSS accelerometer is measured with accuracy better than 0.002 rad (0.1 deg), maximum error with respect to the Sloshsat FLEVO coordinate system.

The location accuracy in the Sloshsat coordinate system is not the relevant error measure for the assessment of data from the accelerometer arrangement. For these, the errors in the distances between the sensors and the relative attitudes of the sensitive axes apply. Thus, the accuracy of the measurement table, better than 0.01 mm, should be taken as a measure of the uncertainty in the geometry of the arrangement. The location of points determined with respect to the arrangement will then have accuracy better than 1 mm maximum in the Sloshsat coordinate system.

The accelerometers are of the Q-Flex family [17], type Allied Signal QA-3000-010, and came with factory-determined bias and gain values, and with correction factors for temperature effects. Each sensor is identified by the direction of its sensitive axis followed by its number in Fig. 2, viz., $Y1$, $Z2$, $X3$, $Z4$, $X5$, and $Y6$. Output is provided in two ranges, ± 1.5 g and ± 30 mg, and the present analysis will deal with the 30 mg range data only. The temperature of each accelerometer and that of the electronics box is determined at a 3 Hz sampling rate. The gyroscopes are Litef μFORS 36/6, and, although these sensors are noisy, stationary rates can be determined accurately from a long averaging period. The MSS sensors are sampled at 30 Hz; the accelerometer signals are passed through a low-pass filter with cutoff at 3 Hz.

Sloshsat FLEVO Data Preprocessing

The data received at the ground station are separated in low speed frame (LSF) and medium speed frame (MSF) data. The LSF data are a subset of the MSF data and are used to monitor Sloshsat performance in (near) real time. The MSS data are input to a Matlab suite of programs, collectively designated "Sloshpost," for validation, correction, conversion to engineering units, formatting, and generation of plots that show time histories [18]. The received data are converted from counts to meters per second squared, and are finally corrected to a_{out}, as in the formula

$$a_{\text{out}} = b_4(T) + \text{SF}_4(T)a_{\text{in}} = a_n + a_{\text{err}} \tag{1}$$

where subscript 4 on the symbols b for bias and SF for scale factor means that these are fourth-order polynomials in sensor temperature T, a_n is the nominal, true value, and a_{err} is the error. Much more elaborate input–output models are in use but the present equation is common and, with some additional corrections to bias and scale factor, was found to be satisfactory for the analysis.

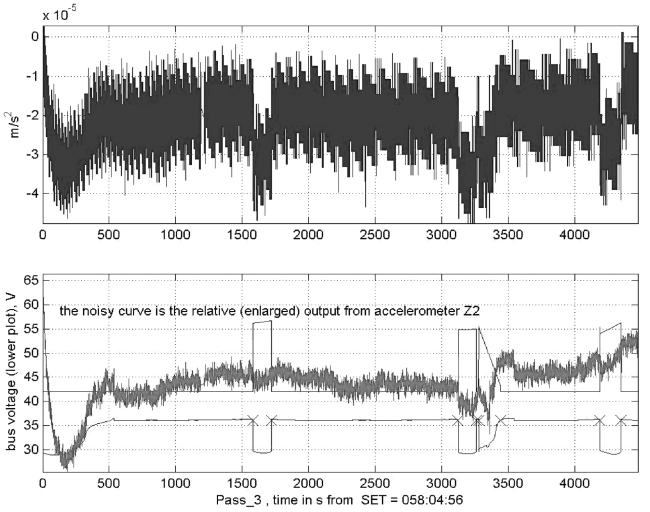

Fig. 3 Record of accelerometer $Z2$ with spikes removed (upper part) and after correction for voltage dip and filtered (lower part).

A typical time series of accelerometer output as provided by Sloshpost, but with some spikes removed, is plotted in the upper part of Fig. 3. The plot shows the effect of the initial heating of the accelerometer at switch-on, which lasts about 500 s, and also some dips that correlate with a drop in bus voltage. The voltage drop is caused by the absence of solar array on the $-Z$ side of Sloshsat, the side of the mating with ESAject. If this side is illuminated by the sun, the exposed solar array area drops and so does the voltage. Another cause of voltage drop is activation of a pressure valve, and this effect is displayed as well, at about $t = 3250$ s (tank C open). Bus voltage drop effects are visible also in other MSF data, notably in temperature sensor records. The accelerometer data are corrected for voltage drop by a shift of signal over the interval of the drop. The magnitude of the shift is determined by the difference in the average output on either side of the edges of the drop interval. An illustration of the amount of shift is shown in the lower part of Fig. 3. A last preprocessing correction, illustrated also, results in a much lower noise level and is effected by passing the signal through a 64-window Hamming or Hanning filter [19]. The width of the window corresponds to a time period of $64/30$ s and was chosen somewhat arbitrarily after comparison of several alternatives. There is little difference between Hamming or Hanning weighting. The use of the filter here is limited to data that nominally are almost stationary.

Calibration Data Selection

The complete history of gyroscope data has been reviewed for periods of near-constant value and in the absence of thruster activity. These periods were first divided into a number of intervals of about 250 s but finally ranged from 150 to 1500 s to cover an integer number of nutation periods, if feasible, and not be too numerous. Altogether, 230 intervals have been selected, and the averaged spin rate has been plotted with the pass number in Fig. 4. For an illustration, Fig. 5 shows actual values during pass_08 from which periods for averaging have been taken. In fact, gyro output is plotted but, as noted already, the gyro axes are close to the principal axes directions. The plot of the angular rate magnitude nearly coincides with the plot of its major component, the spin rate. The disturbance from slosh after thruster activation is clearly shown, e.g., after torques with thrusters $Z2$–$Z3$ about the Y_s ($\sim$ major) axis. Nutation and its decay can be observed as well.

Truly uniform spin rate is obtained only after damping of Sloshsat nutation, at about $\Omega/3$, and slosh effects. The slosh period is about 60 s and damping occurs within five oscillations. Both nutation and slosh damping are exhibited in Fig. 5. The overshoot in rate from the lagging transfer of angular momentum to the liquid in the tank is also shown. Such overshoot and other initial transients have been excluded by specification of the period of near-uniform rate. A

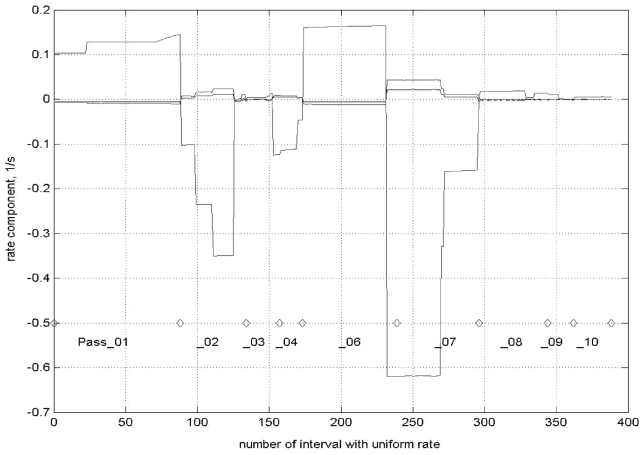

Fig. 4 Periods with uniform rotation rate during the Sloshsat mission.

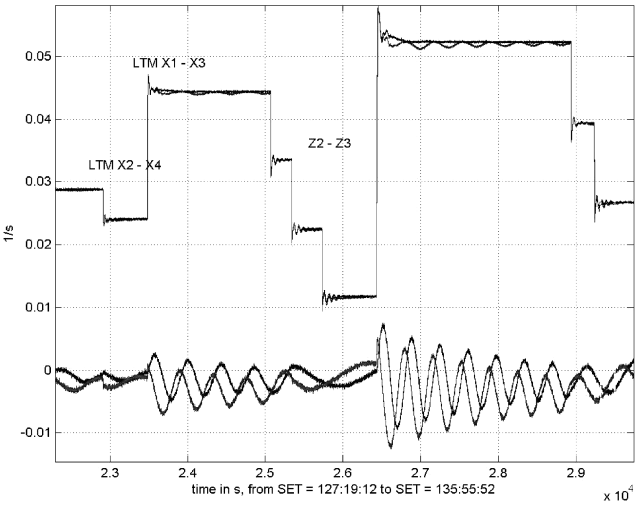

Fig. 5 Gyroscope output during $\sim$2 h of pass_08, with stable spin intervals.

mission anomaly is the leakage of nitrogen propulsion gas from the high-pressure circuit following the opening of tank B during pass_01. Its maximum effect on spin rate, at the maximum high-pressure transducer (HPT) value, is observable in Fig. 4. For the selected periods of near-uniform rate, the gyro output has been matched using least squares to the analytical function determined from the solution of the Euler equation and the mean angular acceleration is estimated.

The preprocessed accelerometer data for the 230 intervals, with the mean angular rate and mean angular acceleration for the interval, form the principal part of the database for the in-space calibration exercise. Additionally, housekeeping data as required, e.g., temperatures and pressure (interval averages), have been included in this database.

Theory

The calibration of the Sloshsat system uses information from rigid body dynamics, which requires integration of Euler's equations, and information from kinematics, viz., knowledge of the acceleration field in a moving coordinate system. Euler's equations are integrated in the principal axes system and the equations are ordered 1, 2, 3, along minimum, intermediate, and major axes, respectively.

Integration of Euler's Equations

In the principal axes coordinate system, the components of the angular rate of a rigid body are written $\boldsymbol{\Omega} = \begin{bmatrix} m_1 & m_2 & (1+m_3) \end{bmatrix}^T W_0$. Euler's differential equations for conservation of angular momentum are

$$\tau_1 = AW_0 m_1' + (C-B)W_0^2 m_2(1+m_3) \tag{2}$$

$$\tau_2 = BW_0 m_2' + (A-C)W_0^2 m_1(1+m_3) \tag{3}$$

$$\tau_3 = CW_0 m_3' + (B-A)W_0^2 m_1 m_2 \tag{4}$$

where $A < B < C$ and $W_0 =$ constant.

At near-uniform spin and small torque $\boldsymbol{\tau}$, $m_i \ll 1$ and $m_1 m_2$ is negligible in the equation for m_3, although a constant value can be incorporated in the spin acceleration $W_0 m_3'$, together with τ_3/C.

Defining $m = W_0 m_1/E_1 + iW_0 m_2/E_2$ and $\psi = \tau_1/(AE_1) + i\tau_2/(BE_2)$, where $E_1 = [BW_0/(C-A)]^{1/2}$, $E_2 = [AW_0/(C-B)]^{1/2}$, Eqs. (2) and (3) are written as $m' = in(1+m_3)m + \psi$, with solution

$$m = e^{inu}[m(0) + \int_0^t \psi(x) e^{-inu(x)}\,\mathrm{d}x]$$

where

$$u(t) = \int_0^t [1 + m_3(x)]\,\mathrm{d}x$$

and n is the nutation rate $W_0^2/(E_1E_2)$.

For constant small torque $\psi = \psi_0 e^{i\varphi} =$ constant, $m_3 = 2at$ and $u = t + at^2$ with $au \ll 1$, so that

$$\int_0^t \psi(x) e^{-inu(x)}\,\mathrm{d}x = i\psi_0 e^{i\varphi}[(1 - au + ia/n)e^{-inu} - 1 - ia/n]/n + \text{terms}\,\mathcal{O}(a^2)$$

For variable torque, the integration would become more complicated but solutions can be found in the literature [12]. The leakage torque is taken as constant because the system pressure drop rate is small, and also the viscous torque contribution is assumed constant because the nutation magnitude is small.

Using real expressions only, the angular rate components given by the approximate solution are

$$\begin{aligned} \Omega_1(t) &= E_1[c_{11} + c_{21}u + c_{31}\cos(nu) - c_{32}\sin(nu)] \\ \Omega_2(t) &= E_2[c_{12} + c_{22}u + c_{32}\cos(nu) + c_{31}\sin(nu)] \\ \Omega_3(t) &= W_0(1 + 2at) \end{aligned} \tag{5}$$

Define $\alpha = \tan^{-1}(n/a)$, $m_0 = |m(0)| = [(\Omega_1(0)/E_1]^2 + [\Omega_2(0)/E_2)^2]^{1/2}$, and $u_0 = \tan^{-1}[r\Omega_1(0)/\Omega_2(0)]$, $r = E_1/E_2$ to write the constants as

$$\begin{aligned} c_{11} &= -(\psi_0/n^2)(n^2+a^2)^{1/2}\cos(\varphi - \alpha) \\ c_{12} &= -(\psi_0/n^2)(n^2+a^2)^{1/2}\sin(\varphi - \alpha) \\ c_{21} &= (a\psi_0/n)\sin\varphi \qquad c_{22} = -(a\psi_0/n)\cos\varphi \\ c_{31} &= m_0\cos(nu_0) - c_{11} \qquad c_{32} = m_0\sin(nu_0) - c_{12} \end{aligned} \tag{6}$$

Note that the magnitudes of $\Omega_1(t)$ and $\Omega_2(t)$ remain constant if $a = 0$. Torque components τ_1 and τ_2 act to turn the rate vector a bit, and have some effect on the spin acceleration via c_{11} and c_{12}:

$$\begin{aligned} \tau_1 &= AE_1 n^2(-ac_{11} + nc_{12})/(n^2+a^2) \\ \tau_2 &= -BE_2 n^2(nc_{11} + ac_{12})/(n^2+a^2) \\ \tau_3 &= 2aCW_0 + (B-A)W_0^2 c_{11}c_{12}/n \\ &\quad + \text{time-dependent negligible terms} \end{aligned} \tag{7}$$

Relations can be derived also with coefficients c_{2i} but these were found to be of no practical use.

The formulas are verified via comparison with a numerical integration of Euler's equations for a Sloshsat-like system. For torques $\mathcal{O}(0.01\ \mathrm{N\cdot m})$, larger than in effect during the operational periods considered, the two solutions are nearly indistinguishable.

The mean values of the rate components over an integer number N of nutation cycles removes the nu modulation but does show the effect of the torque, viz., to first order

$$\begin{aligned} \Omega_{1,\mathrm{mean}} &= E_1(c_{11} + \pi c_{21}N/n) \\ \Omega_{2,\mathrm{mean}} &= E_2(c_{12} + \pi c_{22}N/n) \\ \Omega_{3,\mathrm{mean}} &= W_0(1 + 2\pi aN/n), \end{aligned} \tag{8}$$

an equation useful for the determination of a

Identification of Inertia Tensor and Torque

The Sloshsat inertia tensor is known in the tank axes coordinate system as $J_{3\times3} = \mathbf{Q}\mathrm{diag}(A,B,C)\mathbf{Q}^T$, where orthogonal matrix $\mathbf{Q}$ gives the orientation of the principal axes in the tank axes system. Denoting the coefficients of the angular rate components along the tank axes by $[a_{ij}]$ (determined by least-squares match to the rate data), then the coefficients for the rate along the principal axes become $\mathbf{Q}^T[a_{ij}] = [\alpha_{ij}]$. Because $\mathbf{Q}$ is only approximately correct, the relation to the true components along the principal axes, expressed in c_{ij} as introduced in Eqs. (5), is

$$[\alpha_{ij}] = \mathbf{U}\mathrm{diag}(E_1,E_2,W_0)\begin{bmatrix} c_{31} & -c_{32} & c_{21} & c_{11} \\ c_{32} & c_{31} & c_{22} & c_{12} \\ 0 & 0 & 2at/u & 1 \end{bmatrix} \tag{9}$$

where $\mathbf{U} \sim \mathbf{1}_{3\times3} + \{\boldsymbol{\varepsilon}\}$, $\boldsymbol{\varepsilon}^T\boldsymbol{\varepsilon} \ll 1$.

$\mathbf{U}$ is an unknown orthogonal matrix close to the identity matrix $\mathbf{1}_{3\times3}$ and represents the error in $\mathbf{Q}$. Each row of coefficients α_{ij} is sorted like c_{ij} in sequence of functions $\cos(nt)$, $\sin(nt)$, t, and 1, and, therefore

$$\begin{aligned} [\alpha_{ij}] &= \begin{bmatrix} \alpha_{31} & \alpha_{41} & \alpha_{21} & \alpha_{11} \\ \alpha_{32} & \alpha_{42} & \alpha_{22} & \alpha_{12} \\ \alpha_{33} & \alpha_{43} & \alpha_{23} & \alpha_{13} \end{bmatrix} \\ &= \begin{bmatrix} E_1 & -\varepsilon_3 E_2 & \varepsilon_2 W_0 \\ -\varepsilon_3 E_1 & E_2 & -\varepsilon_1 W_0 \\ -\varepsilon_2 E_1 & \varepsilon_1 E_2 & W_0 \end{bmatrix}\begin{bmatrix} c_{31} & -c_{32} & c_{21} & c_{11} \\ c_{32} & c_{31} & c_{22} & c_{12} \\ 0 & 0 & 2at/u & 1 \end{bmatrix} \end{aligned} \tag{10}$$

Comparison of terms on each side of the equality sign yields 12 equations for three unknown components of $\boldsymbol{\varepsilon}$, six coefficients c_{ij}, E_1, E_2, acceleration a, and rate W_0, i.e., thirteen unknowns. For the short time intervals considered here take $t/u = 1$. Known from the data is also nutation rate n whose expression in E_1, E_2, and W_0 supplies the thirteenth equation. It was found that c_{21} and c_{22} cannot be resolved accurately except for simulated exact data. The equations to be solved are conveniently formulated using a special 2×2 matrix, viz., $A2(x,y)$ with property $A2^TA2 = (x^2+y^2)\mathbf{1}_{2\times2}$ and $A2/(x^2+y^2)^{1/2}$ is orthogonal. This feature allows using singular value decomposition (svd) as a solution method.

Define

$$[\alpha_{ij}]_{2\times2} = \begin{bmatrix} \alpha_{31} & \alpha_{41} \\ \alpha_{32} & \alpha_{42} \end{bmatrix}$$

and obtain from Eq. (9) or (10)

$$\begin{bmatrix} \varepsilon_2 & \varepsilon_1 \end{bmatrix} = \begin{bmatrix} -\alpha_{33} & \alpha_{43} \end{bmatrix}[A2(c_{31},-c_{32})\mathrm{diag}(E_1,E_2)]^{-T} \tag{11}$$

$$\begin{bmatrix} \alpha_{11} & \alpha_{12} \end{bmatrix} + W_0\begin{bmatrix} -\varepsilon_2 & \varepsilon_1 \end{bmatrix} = \begin{bmatrix} c_{11} & c_{12} \end{bmatrix}\mathrm{diag}(E_1,E_2)A2(1,\varepsilon_3) \tag{12}$$

$$[\alpha_{ij}]_{2\times2} = A2(1,-\varepsilon_3)\mathrm{diag}(E_1,E_2)A2(c_{31},-c_{32}) \tag{13}$$

$$\alpha_{13} = W_0 - \varepsilon_2 E_1 c_{11} + \varepsilon_1 E_2 c_{12} \tag{14}$$

$$\alpha_{23} = a(W_0 + \alpha_{13}) \tag{15}$$

The solution starts with the svd of $[\alpha_{ij}]_{2\times 2}$. The right-hand side of Eq. (13) identifies orthogonal $A2(1, -\varepsilon_3)/(1 + \varepsilon_3^2)^{1/2}$ which results from the svd, and yields the product $\text{diag}(E_1, E_2)A2(c_{31}, -c_{32}) = A2(1, -\varepsilon_3)^T[\alpha_{ij}]_{2\times 2}/(1 + \varepsilon_3^2)^{1/2}$ in addition to ε_3. By rearrangement of terms, product $A2(c_{31}, -c_{32})\text{diag}(E_1, E_2)$ is found, required to get $\begin{bmatrix} \varepsilon_2 & \varepsilon_1 \end{bmatrix}$ from Eq. (11), and ratio $r = E_1/E_2 = \{B(C - B)/[A(C - A)]\}^{1/2}$ by division of the diagonal terms. With known $\boldsymbol{\varepsilon}$, $\mathbf{U}$ is calculated as an orthogonal matrix. A better value for $\mathbf{Q}$ is $\mathbf{Q}_{\text{new}} = \mathbf{Q}_{\text{old}}\mathbf{U}$ and new values for ε_i are calculated until $\mathbf{U}$ is iterated sufficiently close to the identity matrix $\mathbf{1}_{3\times 3}$. Simulations for the Sloshsat configuration with realistic errors gave final values after three cycles. W_0 follows from Eq. (14) with substitution of Eq. (12) and gives $s = n/W_0 = [(C - A)(C - B)/(AB)]^{1/2}$. Parameters r and s determine updated values of A and B as a fraction of C by $A/C = (r - s)/[r(1 - s^2)]$ and $B/C = (1 - rs)/(1 - s^2)$. Then E_1 and E_2 are calculated and c_{11} and c_{12} from Eq. (12). Remaining unknowns are solved from Eqs. (6). Differentiation of A/C and B/C with respect to r and s shows that the changes in A/C and B/C are of the magnitude of changes in r and s. The rate values and the torque components are obtained from Eqs. (5) and (7).

Rotation of an Accelerometer Arrangement

The scalar datum from a linear accelerometer with sensitive direction $\boldsymbol{s}$ and its seismic point at location $\boldsymbol{R}$ is given by

$$a_n = \boldsymbol{s}^T\boldsymbol{\sigma}(\boldsymbol{R}) = \boldsymbol{s}^T\boldsymbol{\sigma}(\mathbf{0}) + \boldsymbol{s}^T(\{\boldsymbol{\Omega}\}^2 + \{\boldsymbol{\Omega}'\})\boldsymbol{R} \tag{16}$$

The determination of vectors $\boldsymbol{s}$ and $\boldsymbol{R}$, i.e., the geometry of the MSS, in the tank coordinate system has been discussed already. Acceleration $\boldsymbol{\sigma}(\mathbf{0})$ requires to specify the c.m. of the Sloshsat system as the origin $\mathbf{0}$, which is at location $\boldsymbol{d}_C$ in the tank coordinate system. In absence of thrust and drag forces $\boldsymbol{\sigma}(\mathbf{0}) = \mathbf{0}$ and its location stays put with the water in hydrostatic equilibrium. The centrifugal acceleration output a_{cf} is then given by $\boldsymbol{s}^T\{\boldsymbol{\Omega}\}^2(\boldsymbol{d}_C - \boldsymbol{R}) = a_n - \boldsymbol{s}^T\{\boldsymbol{\Omega}'\}(\boldsymbol{d}_C - \boldsymbol{R}) = a_{\text{cf}}$.

For a period of a few nutation cycles, the time series a_{cf} is constructed from the preprocessed accelerometer output that is averaged, minus the small $\boldsymbol{s}^T\{\boldsymbol{\Omega}'\}(\boldsymbol{d}_C - \boldsymbol{R})$ term calculated from gyroscope data, and the predicted value $\boldsymbol{d}_M$ for $\boldsymbol{d}_C$. The averaging over the nutation cycles changes $\boldsymbol{\Omega}$ to $\boldsymbol{\Omega}_{\text{mean}}$. The objective is to determine the values of $\boldsymbol{\Omega}_{\text{mean}}$ and $\boldsymbol{d}_C$ that provide the best match to a_{cf} for all accelerometers.

Introduce $\boldsymbol{\Omega}_{\text{mean}} = \boldsymbol{W} + d\boldsymbol{\Omega}$ where $\boldsymbol{W}$ is a known (gyroscopes) approximate value of $\boldsymbol{\Omega}_{\text{mean}}$ and $d\boldsymbol{\Omega}$ its unknown error. Similarly, $\boldsymbol{d}_C = \boldsymbol{d}_M + d\mathbf{d}$ with $\boldsymbol{d}_M$ a predicted location of the system c.m. and $d\mathbf{d}$ the error. Consider that the error has a much smaller magnitude than its parent quantity, i.e., the known values are approximately correct. Substitution yields

$$\begin{aligned} a_{\text{cf}} &= \boldsymbol{s}^T\{\boldsymbol{\Omega}\}^2(\boldsymbol{d}_C - \boldsymbol{R}) = \boldsymbol{s}^T\{\boldsymbol{W} + d\boldsymbol{\Omega}\}^2(\boldsymbol{d}_M + d\mathbf{d} - \boldsymbol{R}) \\ &= \boldsymbol{s}^T\{\boldsymbol{W}\}^2(\boldsymbol{d}_M - \boldsymbol{R}) - \boldsymbol{c}_M^T d\boldsymbol{\Omega} + \boldsymbol{s}^T\{\boldsymbol{W}\}^2 d\mathbf{d} \\ &\quad + \text{higher order terms} \end{aligned} \tag{17}$$

where vector $\boldsymbol{c}_M^T = \boldsymbol{s}^T\{\boldsymbol{W}\}\{\boldsymbol{d}_M - \boldsymbol{R}\} + (\boldsymbol{d}_M - \boldsymbol{R})^T\{\boldsymbol{W}\}\{\boldsymbol{s}\}$.

The equation is specialized for each of the six accelerometers and together these can be written as a vector equation. If one introduces vector $\boldsymbol{q}_M$ with components $\boldsymbol{s}^T\{\boldsymbol{W}\}^2(\boldsymbol{d}_M - \boldsymbol{R})$ of each accelerometer, the result is

$$\begin{aligned} \boldsymbol{a}_{\text{cf}} - \boldsymbol{q}_M &= -\mathbf{C}_M d\boldsymbol{\Omega} + \mathbf{S}\{\boldsymbol{W}\}^2 d\mathbf{d} \\ &= \begin{bmatrix} -\mathbf{C}_M & \mathbf{S}\{\boldsymbol{W}\}^2 \end{bmatrix}\begin{bmatrix} d\boldsymbol{\Omega}^T & d\mathbf{d}^T \end{bmatrix}^T \end{aligned} \tag{18}$$

$\mathbf{C}_M$ is the 6×3 matrix of row vectors $\boldsymbol{c}_M^T$, and $\mathbf{S}$ is the 6×3 matrix of row vectors $\boldsymbol{s}^T$.

The 6×6 matrix $\begin{bmatrix} -\mathbf{C}_M & \mathbf{S}\{\boldsymbol{W}\}^2 \end{bmatrix}$ has one zero and one near-zero eigenvalue. For a truly rigid system, i.e., without shifting mass, two zero eigenvalues occur because $d\mathbf{d}$ will be independent of $\boldsymbol{W}$. From the dynamics, it is clear that a system c.m. shift along the rate vector direction cannot be resolved, but for Sloshsat there is little uncertainty about this component. The least-squares solution of Eq. (18) gives the values of $d\boldsymbol{\Omega}$ and $d\mathbf{d}$.

Correction of Bias and Gain of the Accelerometers

If the corrections of the accelerometer signals were perfect, the recovered angular rate and c.m. location would show random errors only. Imperfect correction shows up in systematic errors and these can be used to improve the calibration parameters. The correction equation for one accelerometer is

$$a_{\text{out}} = b_4(T) + \text{SF}_4(T)a_{\text{in}} = a_n + a_{\text{err}} = a_n + \hat{a}_{\text{err}} + \text{white noise} \tag{19}$$

where $\hat{a}_{\text{err}}$ is the mean value of a_{err} and is related to significant variables by

$$\begin{aligned} \hat{a}_{\text{err}} &= \Delta_b + \Delta_\alpha T + \Delta_\beta T_b + \Delta_\pi \text{HPT} + \Delta_\sigma a_p \\ &= \begin{bmatrix} 1 & T & T_b & \text{HPT} & a_p \end{bmatrix}\begin{bmatrix} \Delta_b & \Delta_\alpha & \Delta_\beta & \Delta_\pi & \Delta_\sigma \end{bmatrix}^T \end{aligned} \tag{20}$$

a_p is a predicted accelerometer reading and error vector $\boldsymbol{\Delta} = \begin{bmatrix} \Delta_b & \Delta_\alpha & \Delta_\beta & \Delta_\pi & \Delta_\sigma \end{bmatrix}^T$ has components that express the dependence on the listed variables. Component Δ_σ is a scale factor correction, the others correct the bias value. For the known states in the database with 230 intervals of nearly uniform rates, the values of a_{err}, T, T_b, HPT, and a_p are known and the systematic error vector $\boldsymbol{\Delta}$ can be solved by least squares. Evidently, more variables can be included in the equation and tested for relevance by the value of its corresponding $\boldsymbol{\Delta}$ component.

Applications and Results

Sloshsat calibration means quantification of errors in the performance of each MSS sensor, of errors in the location and attitude of a sensor, i.e., in the geometry of the MSS, and of errors in the inertial properties of the spacecraft. In addition, force and torque from leakage are estimated.

Gyroscope Errors

Gyroscope error has been investigated for a long period of uniform rotation before tank B was opened. The mean value determined from the gyroscope output for the period SET (Sloshsat elapsed time) 11:42:58 to SET 13:03:18, i.e., 4820 s, is 0.10428/s and its standard deviation is calculated at 0.000467/s. In the period, 80 revolutions have been performed as determined from the drops in the bus voltage record, with a total deficit of 0.37006 s, or about one discrete period of the 3 Hz voltage data. Over the first 40 revolutions, the mean angular rate is 0.10423/s and the time deficit is 0.037 s; over the last 40, the rate is 0.10433/s and the deficit is 0.333 s. The first and last 10 revolutions (approximate 1800 data) show rate values of 0.10418/s and 0.10436/s, respectively. Although a slight increase in rate is apparent ($2.623 \times 10^{-8} \times$ time in seconds), the gyroscope output is taken as sufficiently precise at 0.10428/s. From this result, and from the finding that the rate iterated from accelerometer data gave only very small adjustment of gyro rate values, it is concluded that no correction is necessary for the gyroscope data.

Accelerometer Errors

The calibration involves several iterations. The error Eq. (18) for the system c.m. location and the angular rate vector is solved by least squares. The zero order solution uses the values of the mean rate and acceleration from the database and the system c.m. location as

Table 1 Standard deviation of the bias value, in 10^{-6} m/s^2, without correction

	Accelerometer					
	*Y*1	*Z*2	*X*3	*Z*4	*X*5	*Y*6
Iterated data	6.73	3.06	2.39	2.22	3.92	5.05
All data	9.52	7.33	18.6	8.37	5.54	6.69

Table 2 Standard deviation of the bias value, in 10^{-6} m/s^2, after three corrections

	Accelerometer					
	*Y*1	*Z*2	*X*3	*Z*4	*X*5	*Y*6
Iterated data	4.81	2.68	1.69	2.23	1.74	4.89
All data	6.28	6.02	5.36	5.94	4.26	5.71

estimated from the hydrostatic equilibrium configuration. The residual errors, 230 for each accelerometer, are used as input $\hat{a}_{\text{err}}$ to Eq. (20). The solution of that system provides the best linear match of the errors to chosen parameters. As candidate parameters have been explored, the bias, scale factor, and temperature of the accelerometer, the MSS electronics box temperature, the HPT output, and the bus voltage. The bus voltage was found irrelevant as a parameter, but the others showed at least a small dependence. Acceleration at the system c.m., notably due to leakage force, has the same component value for accelerometers with the same sensitive direction, and a constant amount will become part of the bias values.

The updated bias and scale factor values are used to correct the accelerometer data in the database and then the whole procedure is repeated, i.e., determination of c.m. location, angular rate, and parameters. As it turned out, no further improvement was achieved after three (sometimes two) consecutive updates.

The performance of each accelerometer is expressed as a standard deviation, which is the magnitude of the average deviation of the sensor output from its predicted value. As a start, the factory values of the bias have been updated by the sensor output at the end of pass_10 after all propulsion gas had been exhausted and the angular rate is almost zero. These corrections vary between near zero and 7×10^{-6} m/s^2. The errors after the first determination of c.m. and angular rate, i.e., before Eq. (20) has been solved, are shown in Table 1.

For each accelerometer, two data are given: for iterated and for all data. The distinction relates to the magnitude of the angular rate; if it is too small, the iteration fails because the correction is no longer small and the c.m. and rate remain at the initially assumed values. Leakage effects are relatively important at the low level of acceleration that goes with low spin rates. Table 2 shows the results after repeated use of Eq. (20).

A plot that illustrates the actual distribution of bias for accelerometer *Z*2 is given as Fig. 6. The data indicated by plus signs are offset from the data indicated by dots (of the same origin) because of different corrections. The force on Sloshsat that induces acceleration at the bias standard deviation level is $\mathcal{O}(5 \times 10^{-4}$ N). The error component values, multiplied by 10^6, in Eq. (20) after three iterations are listed in Table 3.

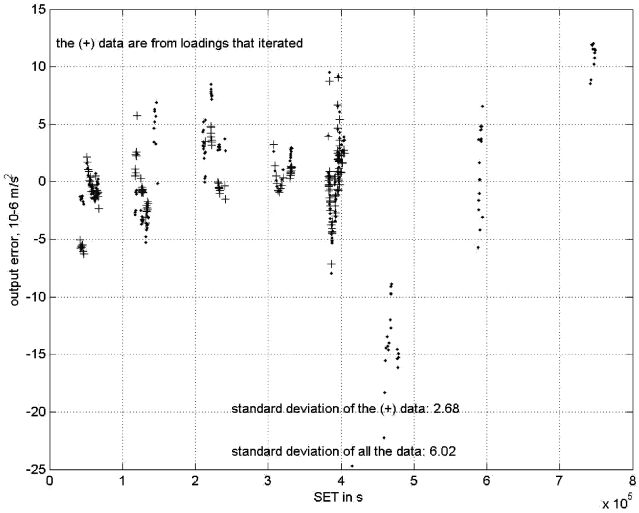

Fig. 6 The difference between predicted and measured data of accelerometer *Z*2.

Hence, as an example, if the output of accelerometer *X*3 is adjusted with a correction of $10^{-6}(100.7 + 0.96T - 5.25T_b - 0.093\text{HPT} - 113.1a_p)$ where variables T, T_b, HPT, and a_p are given their value as determined for each of the 230 intervals of near-uniform rate, the resulting series of 230 data upon comparison with the difference between the predicted and the corrected *X*3 output exhibits a standard deviation of 1.69×10^{-6} m/s^2 (Table 2).

Motion Sensing Subsystem Geometry Errors

The gyroscopes are well aligned with the geometry as embodied in the arrangement of accelerometers and only errors in that geometry are addressed. The equation for the nominal accelerometer signal contains geometric variables $\boldsymbol{R}$ and $\boldsymbol{s}$. The unit vector $\boldsymbol{r}$ along location vector $\boldsymbol{R} = R\boldsymbol{r}$ is used to form vector $\sin\varphi\boldsymbol{t} = \{\boldsymbol{s}\}\boldsymbol{r}$ and it is noted that $\varphi \neq 0$. A triad of orthonormal vectors $\mathbf{Q} = \begin{bmatrix} \boldsymbol{s} & \boldsymbol{t} & \{\boldsymbol{s}\}\boldsymbol{t} \end{bmatrix}$ is formed, and the components of a vector in this triad are indicated with subscripts 1, 2, and 3, respectively. The misalignment of this triad with a known reference triad $\mathbf{Q_0}$ is given by $\mathbf{Q_0} = \mathbf{QU}$, with orthogonal matrix $\mathbf{U} \sim \mathbf{1}_{3\times3} - \{\boldsymbol{\varepsilon}\}$ for small $\boldsymbol{\varepsilon}$. If the error in R is δ, the error in φ is θ and $\boldsymbol{\sigma}_0$ the acceleration at $\boldsymbol{R} = \mathbf{0}$ then the difference between the actual accelerometer data a_n and the predicted value a_p becomes [5]

$$a_n - a_p = \begin{bmatrix} \delta & \theta & \varepsilon_1 & \varepsilon_2 & \varepsilon_3 \end{bmatrix} \cdot \begin{bmatrix} -\sin\varphi(\Omega_2' + \Omega_1\Omega_3) - \cos\varphi\left(\Omega_2^2 + \Omega_3^2\right) \\ R\left[-\cos\varphi(\Omega_2' + \Omega_1\Omega_3) + \sin\varphi\left(\Omega_2^2 + \Omega_3^2\right)\right] \\ R\sin\varphi(\Omega_3' - \Omega_1\Omega_2) \\ \sigma_{01} + R\left[2\cos\varphi\Omega_1\Omega_3 - \sin\varphi\left(\Omega_3^2 - \Omega_1^2\right)\right] \\ -\sigma_{02} - R[\sin\varphi(\Omega_1' - \Omega_2\Omega_3) + 2\cos\varphi\Omega_1\Omega_2] \end{bmatrix} \tag{21}$$

From the metrology report [16] of the MSS geometry, the absolute magnitude of components $\begin{bmatrix} \delta & \theta & \varepsilon_1 & \varepsilon_2 & \varepsilon_3 \end{bmatrix}$ is 10^{-3} m or

Table 3 Error coefficients, ×10^6, for the accelerometer output correction

	Accelerometer					
Coefficient	*Y*1	*Z*2	*X*3	*Z*4	*X*5	*Y*6
Δ_b	18.52	−7.01	100.7	−14.23	−22.72	−29.60
Δ_α	2.29	1.35	0.96	0.52	1.69	2.13
Δ_β	−4.79	−3.14	−5.25	−0.11	−2.00	−2.16
Δ_π	−0.038	0.031	−0.093	0.051	−0.032	0.049
Δ_σ	3271	−220.8	−113.1	264.3	56.9	−3703

2×10^{-3} rad. The magnitude of R is $\mathcal{O}(0.5)$ m, or $\begin{bmatrix} \theta & \varepsilon_1 & \varepsilon_2 & \varepsilon_3 \end{bmatrix} R = [\mathcal{O}(10^{-3})]$ m, and so Eq. (21) shows that the absolute error of a single accelerometer readout is a sum of terms with magnitude $\Omega^2 \times 10^{-3}$ m/s^2 at most, and its likely value (1σ) can be estimated at $\mathcal{O}(10^{-5}$ m/s$^2)$ for $\Omega = 0.2$ rad/s and negligible σ_0. If each accelerometer in the MSS had errors of this magnitude from geometrical causes, the iteration procedures as used for the calibration would result in an error lower than the estimated $\mathcal{O}(10^{-5}$ m/s$^2)$. This is because the geometry of the arrangement is implicitly determined as an average of the actual configurations of the accelerometers, or as remarked already, the relative magnitude of the metrology errors is the pertinent datum. The standard deviation of the bias as determined at $\mathcal{O}(5 \times 10^{-6}$ m/s$^2)$ will not be sensibly affected by the geometrical errors except possibly for high rate values.

Center of Mass Location and Angular Rate Vector

The iterated values of the system c.m. coordinates have been plotted against the iterated spin rate magnitude in Fig. 7 where com (1), (2), and (3) refer to values along X_S, Y_S, and Z_S, respectively. An approximation to the component's data by a curve with few parameters has been included. To start the iteration with Eq. (18), different estimates of the c.m. have been used. Value $\begin{bmatrix} 0.0111 & 0.0001 & -0.1413 \end{bmatrix}^T$ m was predicted by CFD program ComFlo from the final state of a simulation run at 4 rpm [20]. Another value, $\begin{bmatrix} 0.0129 & 0.0005 & -0.1341 \end{bmatrix}^T$, was calculated by elementary integration of mass elements under the assumption that the liquid free surface is flat. The difference in initial condition did not affect the end result of the iteration. As was noted already, iteration is not possible for near-zero spin rates and no points have been plotted in that region. The starting value for the rate vector was taken from the calibration database. It is the averaged gyro output, and it was found that the difference between this spin rate magnitude and the iterated value as generated from the accelerometers output is $<10^{-3}$ rad/s, and mostly $<0.5 \times 10^{-3}$ rad/s, with an occasional spike to 2×10^{-3} rad/s.

Inertia Tensor and Torque

The identification of the inertia tensor starts with the instantaneous angular rate as determined from the accelerometer arrangement. The time series of the rate has been matched by least squares to the functional form [1, u, cos(nu), sin(nu)] that corresponds to the approximate analytical solution of Eqs. (5), Euler's equations. The nutation frequency was determined first and has been used as a known parameter in the matching. An illustration of the goodness of fit to noisy gyro data is provided in Fig. 8, in which a functional form with six coefficients was assumed (of which two proved to have

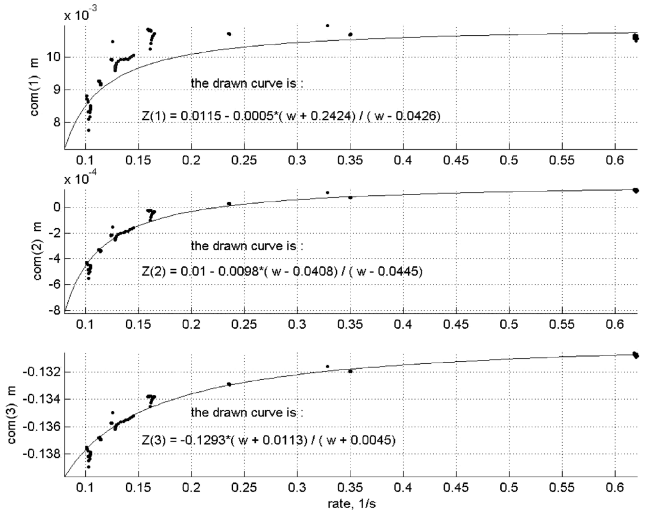

Fig. 7 The Sloshsat system c.m. vs the angular rate magnitude.

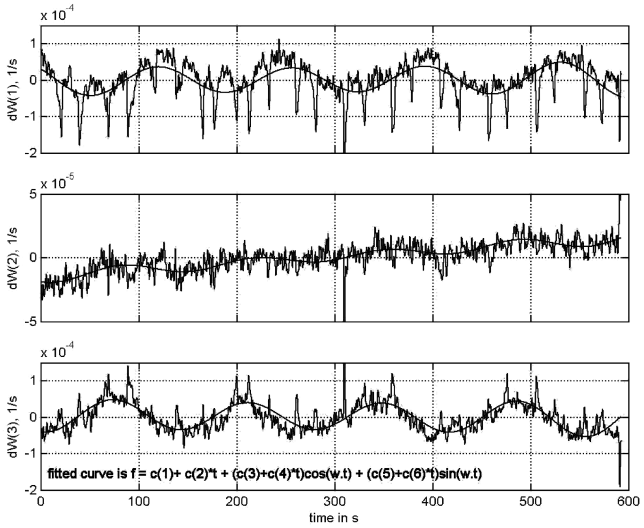

Fig. 8 Modulation of the angular rate just before the opening of tank B.

negligible magnitude). For each of the three rate components, the procedure yields four coefficients a_{ij}. These rate components are along the axes of the tank coordinate system, as embodied in the accelerometer arrangement geometry, but the functional form is the same as for components along the principal axes. The inertia tensor and torque are obtained from a_{ij} via the iterative solution of the variables in Eqs. (9–15). The iteration criterion requires that the difference between the $r = \{B(C-B)/[A(C-A)]\}^{1/2}$ values of two consecutive iteration cycles is less than 10^{-6}. If there is convergence, iteration is fast; often three iterations reduce the difference in r orders of magnitude below the criterion. No convergence is achieved if the nutation components or the spin rate are too low, but also for other conditions, e.g., an inaccurate estimate of the nutation rate. The torque on the system is obtained from Eqs. (7), but the results of simulations indicate that these data are inaccurate. The principal moments of inertia are estimated to be correct to $\mathcal{O}(1\%)$. Simulations of a Sloshsat configuration, using test data contaminated with noise, show the same features as observed during the processing of the actual flight data and verify estimates of accuracy.

Actual data are presented for two states of Sloshsat: case 1 (Table 4) with leakage torque and case 2 (Table 5) without. Each case covers a number of data intervals of three nutation cycles. A comparison between the rate by the matched functions and the rate calculated (by integration of Euler's equations) from the inertia tensor, initial condition, and torque as obtained from the coefficients a_{ij} is shown in Fig. 9 for a typical interval of case 1, and in Fig. 10 for an interval of case 2. The plots start at zero rates because the initial rate values have been subtracted. The sloping line curve corresponds

Table 4 Conditions of case 1

Condition	
Number of intervals	11
Spin rate, rad/s	−0.1617–−0.1585
Nutation magnitude, rad/s	3×10^{-3}–3.7×10^{-4}
HPT, bar	83

Table 5 Conditions of case 2

Condition	
Number of intervals	7
Spin rate, rad/s	+0.1281–0.1283
Nutation magnitude, rad/s	2.6×10^{-3}–3.5×10^{-4}
HPT, bar	0

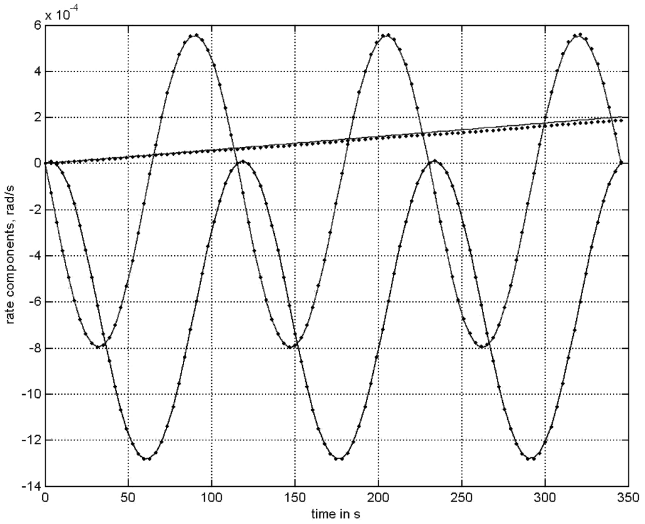

Fig. 9 Fit of experimental data to the calculated (·) data of the identified system.

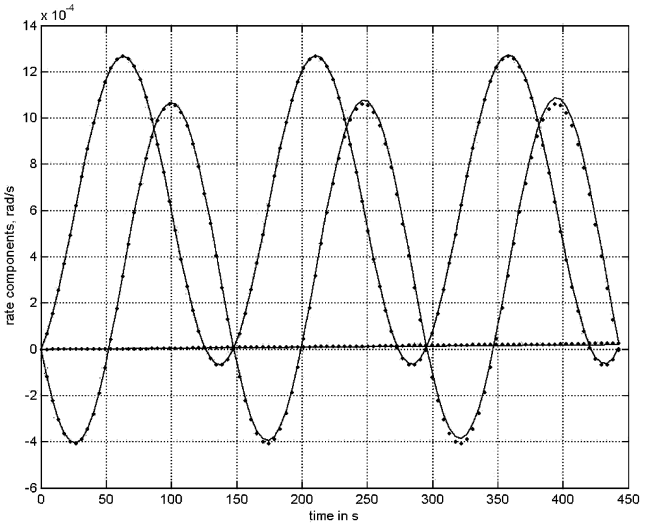

Fig. 10 Fit of experimental data to the calculated data of the identified system without leakage torque.

to the spin rate; the modulated curve of lowest amplitude relates to the rate component along the minimum axis.

The components of the inertia tensor and of the torque in the principal axes system for each interval are shown in Fig. 11. The aggregate results are expressed as mean and standard deviation (std) values. Principal moments of inertia (moi) and torque components along the principal axes are expressed likewise:

$$\text{Case } 1, J_{3\times3}\text{: mean} = \begin{bmatrix} 11.049 & -0.073 & 0.223 \\ -0.073 & 14.499 & -0.234 \\ 0.223 & -0.234 & 10.675 \end{bmatrix}$$

$$\text{std} = \begin{bmatrix} 0.100 & 0.027 & 0.089 \\ 0.027 & 0.001 & 0.018 \\ 0.089 & 0.018 & 0.124 \end{bmatrix} \text{kg} \cdot \text{m}^2$$

$\text{mean}[A\ B\ C] = [10.547\ \ 11.159\ \ 14.516]\,\text{kg}\cdot\text{m}^2$, $\text{std}[A\ B\ C] = [0.081\ \ 0.069\ \ 10^{-15}]\,\text{kg}\cdot\text{m}^2$ mean torque $= [-1.19\ \ 0.48\ \ 0.008]\times 10^{-3}\,\text{N}\cdot\text{m}$, std torque $= [0.48\ \ 0.38\ \ 0.0004]\times 10^{-3}\ \text{N}\cdot\text{m}$.

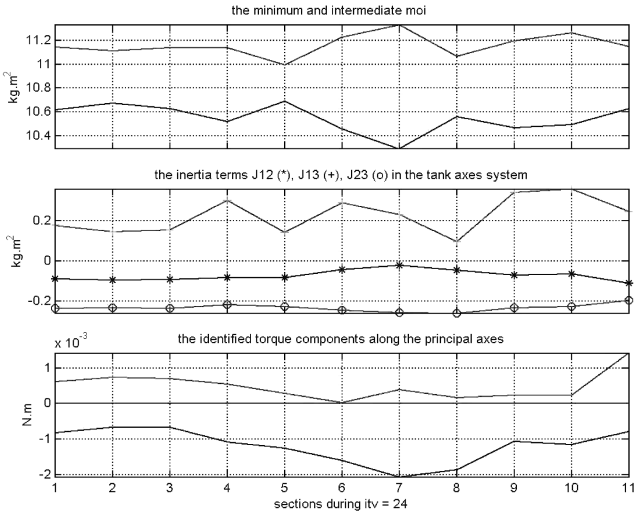

Fig. 11 Identified torque and inertia tensor components from 11 instances of nutational motion.

Similar data for case 2 are as follows:

$$\text{Case } 2, J_{3\times3}\text{: mean} = \begin{bmatrix} 11.219 & -0.112 & 0.088 \\ -0.112 & 14.493 & -0.268 \\ 0.088 & -0.268 & 10.565 \end{bmatrix}$$

$$\text{std} = \begin{bmatrix} 0.109 & 0.023 & 0.116 \\ 0.023 & 0.002 & 0.013 \\ 0.116 & 0.013 & 0.120 \end{bmatrix} \text{kg} \cdot \text{m}^2$$

$\text{mean}[A\ B\ C] = [10.517\ \ 11.245\ \ 14.516]\,\text{kg}\cdot\text{m}^2$, $\text{std}[A\ B\ C] = [0.106\ \ 0.093\ \ 10^{-15}]\,\text{kg}\cdot\text{m}^2$ mean torque $= [-0.27\ \ 0.08\ \ 0.0006]\times 10^{-3}\,\text{N}\cdot\text{m}$, std torque $= [0.36\ \ 0.16\ \ 0.0001]\times 10^{-3}\ \text{N}\cdot\text{m}$.

The relatively large torque in case 1 is mainly by gas leaking from the high-pressure system. If it were due to nutation damping torque from viscous effects, the spin rate magnitude would increase. Major moi C cannot be calculated and is given its value as determined from preflight data. Values of A and B are calculated as fractions of C and will have errors if C has.

For higher spin rates, up to -0.6 rad/s, no significant changes in inertia tensor value are found. This is in agreement with predictions of the inertia tensor of Sloshsat from CFD simulations with ComFlo [20]. The inertial properties of the dry Sloshsat after correction of measured data [1,21] are

$$J_{3\times3\ \text{dry}} = \begin{bmatrix} 8.54 & -0.065 & 0.14 \\ -0.065 & 10.77 & -0.20 \\ 0.14 & -0.20 & 8.73 \end{bmatrix} \text{kg} \cdot \text{m}^2 \qquad (22)$$

and the contribution by hydrostatic liquid is calculated. CFD results [20] differ somewhat from the outcome of an elementary integration assuming a flat free liquid surface. For frozen (no liquid motion) Sloshsat, the resulting system inertia tensors are

$$\text{ComFlo}, J_{3\times3\ \text{frozen}} = \begin{bmatrix} 11.40 & -0.08 & 0.37 \\ -0.08 & 14.70 & -0.24 \\ 0.37 & -0.24 & 10.53 \end{bmatrix} \text{kg} \cdot \text{m}^2$$

$$\text{flat surface}, J_{3\times3\ \text{frozen}} = \begin{bmatrix} 11.78 & -0.06 & 0.35 \\ -0.06 & 14.50 & -0.27 \\ 0.35 & -0.27 & 9.94 \end{bmatrix} \text{kg} \cdot \text{m}^2$$

Leakage Force and Torque

The opening of tank B at SET 17:34:02 was followed by a decrease in HPT value, Fig. 12, and a sloping output from the MSS sensors in Fig. 13. At the dot mark ($\sim$12, 600 s), tank B is opened; the cross (at

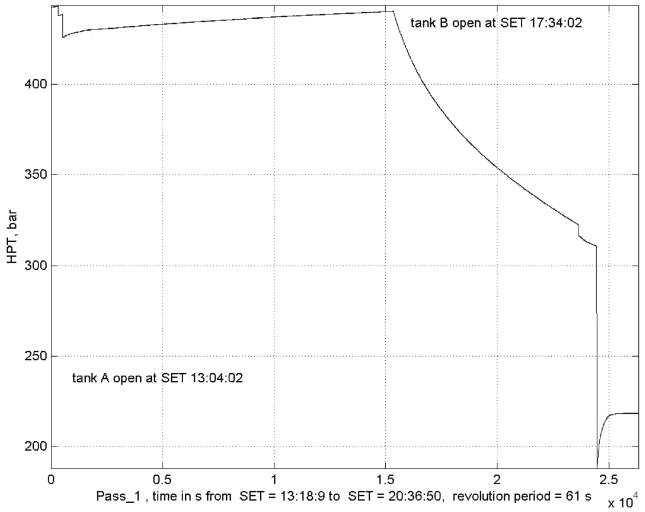

Fig. 12 History of the system high pressure during pass_01, showing the start of leakage upon the opening of tank B.

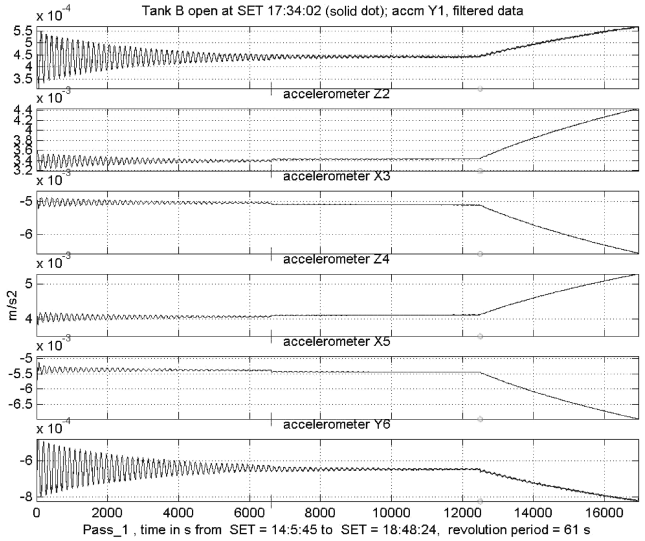

Fig. 13 Accelerometer data during pass_01.

$\sim$6600 s) marks a torque pulse of $1/30''$ by thruster pair $Z1$–$Z4$. The conclusion was that a leak had sprung, later concluded to be in the high-pressure circuit. The torque identified in the previous section is the sum of the torque from leaking gas and the torque from viscous dissipation in the water. Comparison of the slopes of the spin component in Figs. 9 and 10 show leakage torque to be the larger of the two (disregarding a possible effect on torque by the parity of the spin). Both force and torque from leakage are estimated now by various methods.

The linear acceleration from the leakage force has not been accounted for in any of the equations and should therefore show up in parameter Δ_π of Eq. (20), assuming that the leakage force magnitude is related to the HPT value. Disregarding effects from leakage torque on Δ_π, a magnitude of 0.05×10^{-6} (see Table 3) results in a leakage force of 1.3×10^{-3} N at an HPT level of 200 bar. For a different approach, the acceleration resulting from the opening of tank B is estimated. The corrected accelerometer output for a period of 5880 s until tank B was opened has been approximated by a quadratic polynomial in time, and the output just before the opening was determined from the polynomial value. The same procedure for a period of 4500 s from the opening of tank B gave the output just after the opening. By this procedure, the effect of noise on the jump in accelerometer signal is removed. The output jump in the different accelerometers is listed in Table 6.

Table 6 Difference in predicted accelerometer readings before and after the leak

Accelerometer	Difference, 10^{-6} m/s^2
$Y1$	2.8
$Z2$	20.2
$X3$	−26.1
$Z4$	22.0
$X5$	−26.0
$Y6$	−6.4

The force that generates the output jump in Table 6 would have magnitude 4×10^{-3} N, and represents the value of the leakage force at maximum HPT, 440 bar. The X and Z accelerometers show consistent jumps, but the Y accelerometers show a large disparity. However, their output is near zero and therefore not very accurate and subject to torque effects. If the gas were exhausted at the thruster efficiency, it would take at this thrust magnitude about 70 h to deplete all four tanks. The pressure drop rate as recorded in Fig. 12 indicates complete exhaustion after about half the 70 h time span, which can be explained from a low thrust efficiency of the leak.

An interval of four nutation periods just before tank B was opened (Fig. 8) shows $\boldsymbol{\Omega}'_{\text{mean}} = 10^{-8} \times \begin{bmatrix} -11.3 & 5.50 & 3.43 \end{bmatrix}$ s^{-2} and $\boldsymbol{\Omega}_{\text{mean}} = \begin{bmatrix} -0.0045 & 0.1287 & -0.0088 \end{bmatrix}$ s^{-1}. Just after the opening, the values from four nutation periods (550 s) are $\boldsymbol{\Omega}'_{\text{mean}} = 10^{-6} \times \begin{bmatrix} -0.230 & 5.431 & -0.325 \end{bmatrix}$ s^{-2} and $\boldsymbol{\Omega}_{\text{mean}} = \begin{bmatrix} -0.0047 & 0.1303 & -0.0089 \end{bmatrix}$ s^{-1}.

$J_{3\times3}\boldsymbol{\Omega}'$ yields $10^{-5} \times \begin{bmatrix} -0.32 & 7.88 & -0.48 \end{bmatrix}$ N·m as the maximum leakage torque. If all this torque were due to the leakage force, the estimated moment arm is 0.02 m and the contribution of the torque to the accelerometer output is negligible in comparison to the load by the estimated force.

Conclusions

The knowledge of the functional form of the angular rate vector history leads to an accurate determination of the coefficients of the function. The coefficients allow identification of the inertia tensor of the system and of the acting torque. A simulator that integrates Euler's equations was found to be a useful instrument for inspection of the accuracy of the identified parameters.

The alternation between the iteration of variables that are determined by the full MSS data (system c.m. and angular rate) and the determination of parameters of individual accelerometers gave convergent estimates and considerable reduction of unmodeled errors. The 1σ value for the steady signal of an individual accelerometer is estimated $\mathcal{O}(5 \times 10^{-6}$ m/s$^2)$ in the 30 mg range, including the contribution from leakage force variation. The Y accelerometers have the largest uncertainty, due to the low loading and the sensitivity to nutation effects.

The MSS concept of six high-quality accelerometers and three low-cost gyroscopes is attractive. The system is robust by technology and redundancy. Mutual calibration and identification of system parameters is feasible. The locations and attitudes of the sensors are not critical although it is advisable to have the sensitive directions of all accelerometers at a large offset from the major axis of inertia.

The torque from leaking gas can be determined from the buildup of angular rate. The leakage force is more difficult to determine, but the estimates should have the correct order of magnitude because a variety of crosschecks show no contradiction.

The MSS errors of geometric origin are estimated to be of lower magnitude than errors from other causes. Good data on the damping by the liquid of slosh and nutation, as in Figs. 5, 8, and 13, have been recorded and merit detailed interpretation.

Acknowledgments

Sloshsat FLEVO is a joint program between the European Space Agency and the Netherlands Agency for Aerospace Programs. The main contractor is the National Aerospace Laboratory (The

Netherlands), with the participation of Fokker Space (The Netherlands), Verhaert (Belgium), Rafael (Israel), and NASA (United States). The Sloshsat FLEVO development is performed under the framework of the European Space Agency Technology Demonstration Program Phase 2 and the Netherlands Agency for Aerospace Programs Research and Technology program. The Sloshsat data are copyrighted by the European Space Agency and the Netherlands Agency for Aerospace Programs, 2005.

References

[1] Prins, J. J. M., "Sloshsat FLEVO Project, Flight, and Lessons Learned," *Proceedings of the 56th International Astronautical Congress* [CD-ROM], International Astronautical Congress Paper 05-B5.5.05, Oct. 2005.

[2] Vreeburg, J. P. B., "Measured States of Sloshsat FLEVO," *Proceedings of the 56th International Astronautical Congress* [CD-ROM], International Astronautical Congress Paper 05-C1.2.09, Oct. 2005.

[3] Veldman, A. E. P., Gerrits, J., Luppes, R., Helder, J. A., and Vreeburg, J. P. B.,"The Numerical Simulation of Liquid Sloshing on Board Spacecraft," *Journal of Computational Physics*, Vol. 224, May 2007, pp. 82–99. doi:10.1016/j.jcp.2006.12.020

[4] Santiago-Prowald, J., Sanz-Andrés, A., and Bezdenejnykh, N. A., "On-Earth Calibration of Accelerometers for Microgravity Applications," *Microgravity Science and Technology*, Vol. 9, No. 1, 1996, pp. 46–54.

[5] Vreeburg, J. P. B., "Analysis of the Data from a Distributed Set of Accelerometers, for Reconstruction of Set Geometry and Its Rigid Body Motion," *Space Technology and Applications International Forum-1999* [CD-ROM], edited by M. Genk, CP 458, American Inst. of Physics, Melville, NY, 1999, pp. 496–509.

[6] Chen, J.-H., Lee, S.-C., and DeBra, D. B.," Gyroscope Free Strapdown Inertial Measurement Unit by Six Linear Accelerometers," *Journal of Guidance, Control, and Dynamics*, Vol. 17, No. 2, March–April 1994, pp. 286–290.

[7] Tanygin, S., and Williams, T.," Mass Property Estimation Using Coasting Maneuvers," *Journal of Guidance, Control, and Dynamics*, Vol. 20, No. 4, 1997, pp. 625–632.

[8] Peck, M. A.," Mass-Properties Estimation for Spacecraft with Powerful Damping," *AAS/AIAA Astrodynamics Specialist Conference*, American Astronautical Society Paper 99-430, Aug. 1999.

[9] Lee, A. Y., and Wertz, J., "In-Flight Estimation of the Cassini Spacecraft's Inertia Tensor," *Journal of Spacecraft and Rockets*, Vol. 39, No. 1, Jan.–Feb. 2002, pp. 153–155.

[10] Psiaki, M. L., "Estimation of Spacecraft Attitude Dynamics Parameters by Using Flight Data," *Journal of Guidance, Control, and Dynamics*, Vol. 28, No. 4, 2005, pp. 594–603.

[11] Palimaka, J., and Burlton, B. V., "Estimation of Spacecraft Mass Properties Using Angular Rate Gyro Data," *AIAA/AAS Astrodynamics Conference*, TP A92-5205122-13, AIAA Paper 1992-4365, 1992, pp. 21–26.

[12] Tsiotras, P., and Longuski, J. M.," Analytic Solutions for a Spinning Rigid Body Subject to Time-Varying Body-Fixed Torques, Part 2: Time-Varying Axial Torque," *Journal of Applied Mechanics*, Vol. 60, No. 3, 1993, pp. 976–981.

[13] Longuski, J. M., Gick, R. A., Ayoubi, M. A., and Randall, L.," Analytical Solutions for Thrusting, Spinning Spacecraft Subject to Constant Forces," *Journal of Guidance, Control, and Dynamics*, Vol. 28, No. 6, 2005, pp. 1301–1308.

[14] Pivovarov, M. L., Ferreire, L. O., and Lopes, R. V. F., "Rigid Body Rotation Evolution Due to a Disturbing Torque Which is Known in a Body Frame," *Acta Mechanica*, Vol. 133, Nos. 1–4, 1999, pp. 239–246. doi:10.1007/BF01179020

[15] Wilson, E., Lages, C., and Mah, R., "On-line, gyro-based, mass-property identification for thrusters-controlled spacecraft using recursive least squares," *Proceedings of the 45th IEEE International Midwest Symposium on Circuits and Systems*, Vol. 2, Inst. of Electrical and Electronics Engineers, New York, 1992, pp. 324–327.

[16] Willemse, B. B., and Prins, J. J. M., "SLOSHSAT FLEVO PFM Integration Report Alignment and Metrology," National Aerospace Lab. Rept. CR-2001-229, May 2001.

[17] Foote, S. A., and Grindeland, D. B., "Model QA3000 Q-FLEX® Accelerometer High Performance Test Results," *AES Magazine*, June 1992, pp. 59–67.

[18] Willemse, B. B., "Software User Manual for 'Sloshpost': a MATLAB Software Tool for Post Processing Sloshsat FLEVO Medium Speed Frame Data," National Aerospace Lab. Rept. TR-2001-190, April 2001.

[19] Rogers, M. J. B., McPherson, K., Moskowitz, M. E., and Reckart, T., "Accelerometer Data Analysis and Presentation Techniques," Tal-Cut Co. at NASA Lewis Research Center, Rept., Sept. 1997.

[20] Helder, J. A., "Sloshing SloshSat FLEVO: Numerical Simulation of Coupled Solid-Liquid Dynamics in Micro-Gravity," M.S. Thesis, Groningen State Univ., Dept. of Mathematics, Sept. 2005.

[21] Willemse, B. B., "SLOSHSAT FLEVO PFM Inertial Properties Measurements Report," National Aerospace Lab. Rept. CR-2001-185, April 2001.

D. Spencer
Associate Editor